Research article

Consolidation of Cu- and Ti-based metal powders using layer-by-layer, spot pulsed electric current sintering

Abstract

In this paper, we propose a technique for additive manufacturing of bulk materials from electrically conductive powders, based on the method of point wise electro pulse sintering. This method consists of layer-by-layer consolidation of powders, each layer being formed as a result of successive sintering of small portions of powder compressed between the electrode and the substrate, or between the electrode and the previously sintered layer. Using the proposed method, bulk samples were obtained from powders having the different chemical composition (Cu, Ti, mechanically alloyed tin bronze), and particles of various shapes (dendritic, dumbbell, stone-shaped). Using X-ray diffraction, electron microscopy, and micro hardness measurements, the structural phase states, and porosity of the obtained bulk consolidated materials were studied. Sintering of powders using this method is greatly influenced by the heat release along the boundaries of the particles, which in turn depends on the electrical resistivity of the material. The porosity of the sintered samples mainly depends on the type of powder used and decreases with the decreasing size of the powder particles.

Keywords: additive manufacturing, electro pulse sintering, metal powders, porous structure

Elkin IA,[1] Volkov VA,[1] Stolbov KS,[1] Kolodkin DA,[2] Chulkina AA,[1] Beltyukov AN[1]
[1]Udmurt Federal Research Center, the Ural Branch of the Russian Academy of Sciences, Russia
[2]M.N. Mikheev Institute of Metal Physics of the Ural Branch of the Russian Academy of Sciences, Russia

Correspondence: Elkin IA, Udmurt Federal Research Center, the Ural Branch of the Russian Academy of Sciences, 34 T. Baramzina St., Izhevsk, 426067, Russia, Email ivan.a.elki@gmail.com

Abbreviations: LENS, laser engineering net shaping; EBAM, electron beam additive manufacturing; AM, additive manufacturing; CSR, coherent scattering regions

Introduction

Additive manufacturing (AM) has enormous prospects in the modern industry. Thanks to these technologies, it is possible to produce products with a complex shape, as well as to obtain materials with unique complex properties. Presently the most common additive manufacturing methods using metal powders are powder bed fusion (PBF),[1] laser engineering net shaping (LENS),[2] electron beam additive manufacturing (EBAM).[3] Even though these methods are widely used, they are not without drawbacks. The most serious disadvantages include the necessity for complex and expensive equipment, high requirements for the quality of the powders used, as well as the difficulty of obtaining parts without residual porosity and with high surface quality. Residual porosity and roughness can be eliminated by choosing the optimal parameters of the production process,[4,5] which limits the range of materials that can be used.[6] The most commonly used powders are carbon,[7] stainless,[8] high-speed,[9] tool steels,[10] and titanium alloys.[11] Typically, additive technologies are used to produce non-porous materials, but some parts require a porous structure. Currently, an urgent task in the field of additive manufacturing is to obtain materials with a volume gradient of porosity.[12] For example, materials based on Co-Cr[13,14] Ti[15,16] and Ta[17–19] are used as implants. Such implants are better accepted by the human body compared to materials without a porosity gradient. Porous materials based on copper are used as filters, heat (capillary) pipes, and plain bearings. Existing additive manufacturing methods only allow one to obtain materials with restrictions either in shape or in porosity.[20–22]

The range of objects that can be produced by additive manufacturing is extremely wide, so there is a constant search for new methods. The method proposed in this paper can be considered, to some extent, as a development of the pulsed electric current sintering (PECS) method.[23–28] In the conventional PECS method, the entire volume of powder is poured into a dielectric matrix, compressed by electrodes, and a powerful electric current pulse is passed through it. This method allows for obtaining bulk material with a different degree of porosity[29,30] from virtually any electrically conductive powder. The disadvantages of PECS include limits on the shapes of the materials obtained and the requirement for a pressing system and a high-power electric energy source. Additionally, selecting the modes of electro pulse sintering is necessary for each type of powder, since under unstable operating modes, the electric explosion of the powder or inhomogeneous sintering of the powder is possible.[31,32] In the proposed method, the powder is sintered layer-by-layer and each layer is sintered point-by-point. This makes it possible to use a low power pressing system and a low power electric energy source. In addition, during the sintering of powders, we can change the level of mechanical and electrical effects at each sinter point, which ensures the creation of the required porous structure in the volume of the sample. Since this additive manufacturing method is under development, the aim of this work was to study the influence of production modes, materials of used powders, their dispersion and morphology, on the quality of the materials formed.

Materials and methods

Samples were obtained according to the scheme presented in Figure 1. An electrically conductive substrate was placed on the base of a PECS unit to serve as the lower electrode in the electric

circuit. A 0.25mm thick layer of powder was spread over the substrate. Then, the process of sintering was initiated. The flat-ended upper electrode (1mm in diameter) pressed a portion of the powder to the substrate with the pressure of 3MPa; the electric circuit was closed and current passed through the circuit. We used a pulsed AC source with the amplitude of the output voltage of 0.5V and a current of 10A with pulse duration of 20ms to sinter the samples. As a result of the current passage and the compression by the electrode, the powder was sintered and welded to the substrate to form a weld spot 1mm in diameter. Then, the electrode was raised over the powder surface and shifted one step to the right; the electrode pressed another portion of the powder and the current pulse passed through the circuit. The repetition of the procedure resulted in the formation of a "path" in the sintered powder of 10mm in length and 1mm in width. Next, the electrode was shifted to the next line and started to form another "path" adjacent to the first one. Multiple repetitions of the above procedure result in the formation of a sintered layer measuring about 10*10*0.1 mm. To complete the subsequent layer, another portion of the powder was spread over the sintered layer and welded to it in the same way. As such, bulk samples in the form of plates were obtained. To position the electrode in the X-Y plane within the boundaries of the processed layer, as well as to change its height above the processed surface, a computer numerical control (CNC) machine was used. The electrode scanning step ranged between 0.3–0.7mm.
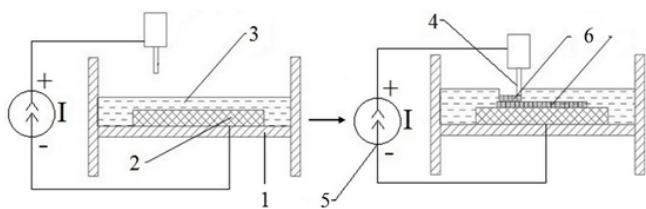

Figure 1 Layer-by-layer spot PECS: on the base of the unit (1) a metal substrate (2) is placed to serve as the lower electrode. 0.25 mm thick layer of powder (3) is spread over the substrate. The powder is pressed to the substrate by the upper electrode rod (4) and is sintered into a spot of 1 mm in diameter by the electric current pulse from the source (5). By the repetition of the procedure sintered layers (6) are formed.

The powders were sintered in air, without a protective atmosphere, at an ambient temperature of 23°C. Because of small heat generation caused by the action of a single current pulse and the high heat conduction of the sample and the powder bed, during powder sintering, there was no noticeable heating of the sample and the electrode. This suggests that the current passage results in heating mainly the contacts between the powder particles and welding the particles along their boundaries. We used a copper electrode (purity 99.9 wt.%). In addition to the copper electrode, we also tested steel (Fe-0.3C wt.%) and tungsten electrodes (99.9 wt.%). However, despite the higher melting temperature of steel and tungsten, they tended to be welded to the sintered layer. The copper electrode was not welded to the sample surface because of the high heat conduction and low electrical resistivity of copper, due to which the electrode was insignificantly heated by the electric current passage, and its melting during the contact with the powder was excluded (Figure 2). To test the proposed technique, we used powders prepared from different metal materials with different structural phase states, different shapes and particle sizes (copper, titanium, and bronze). The copper powder (PMS-1, Cu-0.05Pb-0.018Fe-0.005Sb-0.003As wt.%, made in Russia), obtained by electrolytic deposition, has dendritic particles; the titanium powder (PTM-1, Ti-0.08N-0.05C-0.35H-0.2Fe-0.2Ni-0.1Si wt.%, made in Russia), obtained by the reduction of titanium oxides, has dumbbell-shaped particles; and the bronze powder particles were stone-shaped (Figure 2). The Cu-20wt.% Sn bronze powder was obtained by the mechanical alloying (MA) of copper (PMS-1) and tin powders (purity 99.9 wt.%) in a Fritch Pulverisette-7 planetary ball mill for 18 hours under argon atmosphere. According to electron microscopy, the copper powder particles were 30–50μm in size; the size of the titanium powder particles was in the range of 3–25μm; and the bronze powder particles were about 55μm in size. The electrical resistivity of massive copper, bronze and titanium is $17.5 \cdot 10^{-9}$, $95\text{-}100 \cdot 10^{-9}$ and $600 \cdot 10^{-9}$ Ohm, respectively.[33,34] Copper and MA bronze powders were sintered on the tin substrate (purity 99.9 wt.%), and titanium powder was sintered on steel substrate (Fe-0.3C wt.%). The structural state and phase composition of the samples were studied by X-ray diffraction (MiniFlex 600, Co-Kα radiation) and electron microscopy (Quanta-200). The microhardness was measured using a microhardness tester PMT-3 (made in Russia). Qualitative and quantitative X-ray phase analysis, determination of the size of coherent scattering regions (CSR) were carried out using the Match 3 program and software package.[35] Sample porosity was evaluated by the analysis of electron microscope images using the ImageJ program. For this purpose, the fraction of the dark areas of the total area of the image was determined.
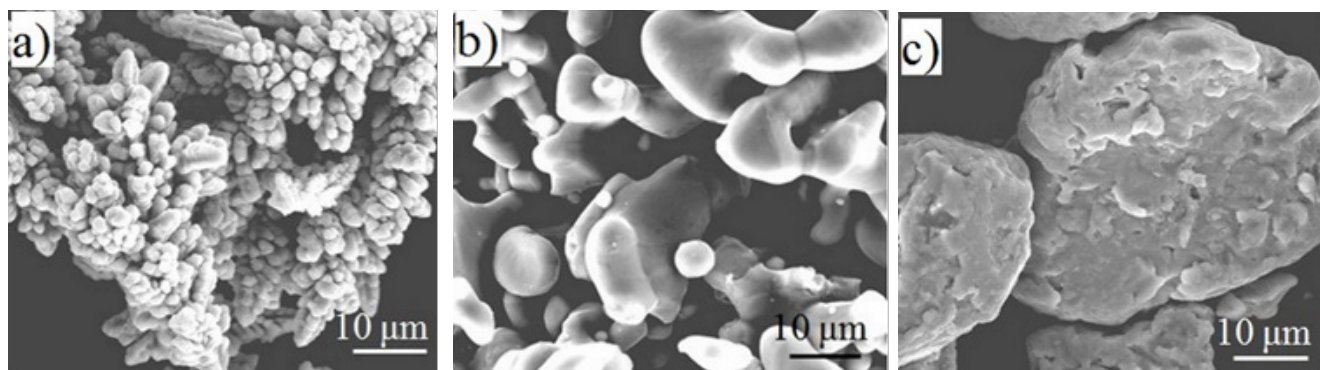

Figure 2 Electron microscope images of initial powders: a – copper with dendritic particles (obtained by electrolytic deposition); b – titanium with dumbbell-shaped particles (obtained by the reduction of titanium oxides); c – bronze with stone-shaped particles (obtained by mechanical alloying).

Results

Porosity and microhardness of the obtained samples

As described above, bulk samples in the form of plates with dimensions of about 10x10x1 mm were obtained from powders of copper (Figure 3A), titanium (Figure 3B) and bronze (Figure 3C). Samples consisted of 10 layers. There were no fundamental difficulties in obtaining samples of greater thickness. It can be seen from the Figure 3 that the samples have no signs of warping and delamination of the sintered layers. In the process of powder consolidation, various powders were welded differently to the substrate. The titanium-based sample was easily detached from the steel substrate because the energy of the electric pulse was insufficient to form a strong bond between the first layers of the sample and the steel substrate. Samples based on copper and bronze were welded to a certain extent to a low-melting (232°C) substrate made of tin, which indicates its partial melting, and because of it, part of the tin penetrated the interior of the porous sample.
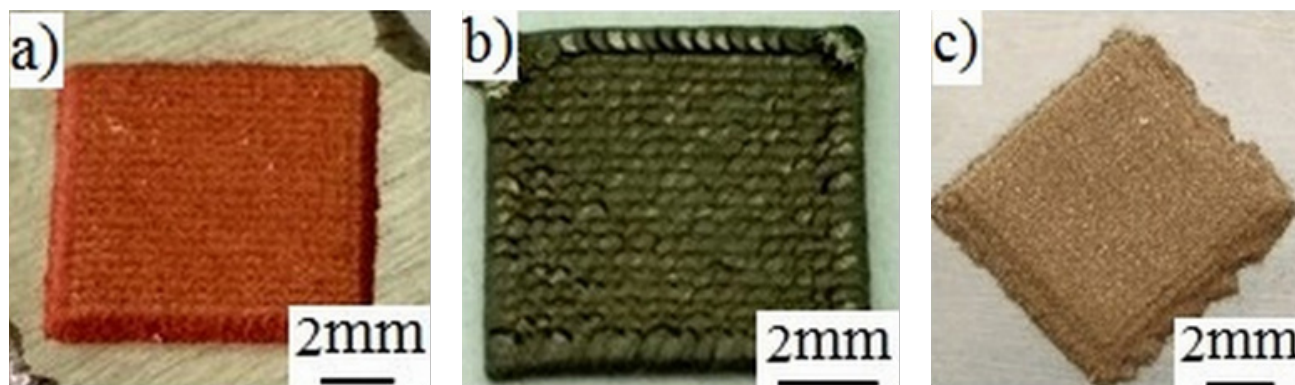

Figure 3 Photos of the samples obtained by layer-by-layer spot PECS from powders of copper (a), titanium (b), MA bronze (c). The samples are in the form of plates measuring 10*10*1 mm, with no signs of warping or delamination, and they do not contain any large defects.

Figure 4 shows the electron microscope images of the sample cross-sections obtained from copper, titanium and bronze powders. The porous structure of the samples can be observed. The porosity values obtained by the analysis of the electron microscope images of the sintered samples are given in Figure 5A. The sample porosity significantly depends on the type of powder used. The titanium-based sample is characterized by the smallest pore size of 2-6μm (Figure 4B), and the porosity is 8-9%. In the lower left-hand corner of the titanium sample image, there is a region with higher porosity, which can be due to the crumbling of some part of the sample in the process of the metallographic specimen preparation, as a result of the incomplete sintering of the sample. The bronze-based sample has the largest pore size of 33-95μm (Figure 4C), and its porosity is 24%. The copper-based sample has pores of 12–30μm in size (Figure 4A), and the highest porosity of 35%. According to the obtained data, the porosity of the samples and the size of the pores increase with the increasing size of the powder particles. At higher magnification (Figure 6) one can see how the powder particles are welded together. Depending on the morphology of the particles and their size, a different number and different lengths of weld areas are observed. In a copper-based sample, due to the dendritic shape of the particles, there is a small number of contacts, and the contacts are short (Figure 6A). In the bronze-based sample, there are also a few contacts, but they are extended since the powder particles are large and irregular in shape (Figure 6C). In the sample prepared from the titanium powder with small dumbbell-shaped particles, the largest contact area between the particles is observed (Figure 6B).
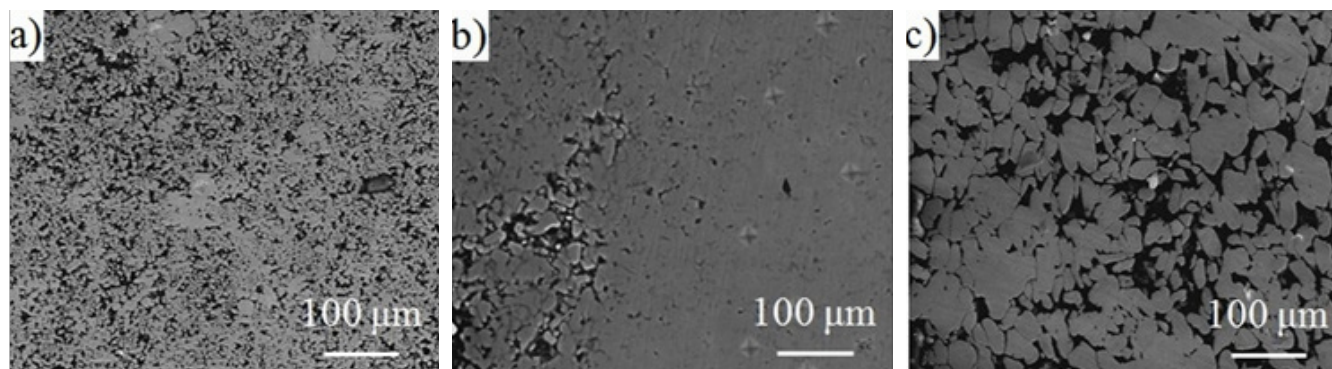

Figure 4 Electron microscope images of the sections of samples obtained by layer-by-layer spot PECS from copper (A), titanium (B) and bronze (C) powders. The porous structure of the samples can be seen in the images.
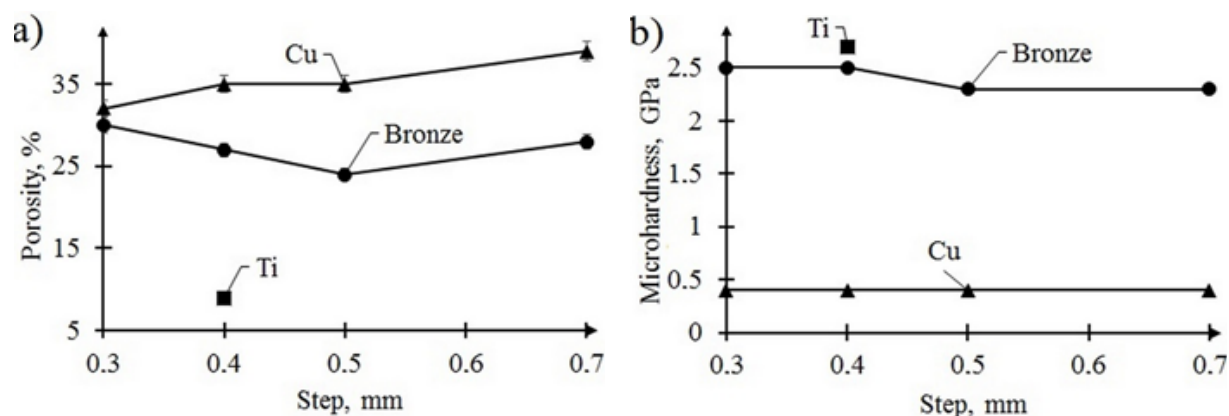
Citation: Elkin IA, Volkov VA, Stolbov KS, et al. Consolidation of Cu- and Ti-based metal powders using layer-by-layer, spot pulsed electric current sintering. *Material Sci & Eng.* 2020;4(1):1–7. DOI: 10.15406/mseij.2020.04.00118

Figure 5 Porosity (A) and microhardness (B) of copper (▲), titanium (■) and bronze (●) samples obtained by layer-by-layer spot PECS of powders with different scanning step.
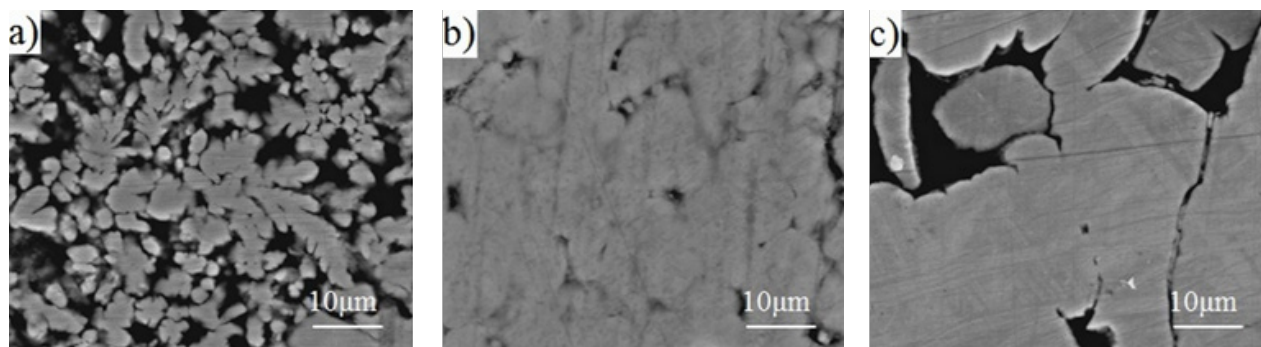

Figure 6 Electron microscopic images of powder particles in sintered samples: in copper (A), in titanium (B), in bronze (C).

The quality of powder sintering can be evaluated by the microhardness of the sintering compacts. Microhardness is determined by the hardness of the powder material, the degree of the particle welding, and the porosity of the sample. Figure 5B shows the microhardness values for the samples obtained from different powders and with different electrode scanning steps. We can see that copper-based samples have the smallest microhardness of 0.4GPa, which is independent of the scanning step. Their microhardness is almost twice as small as that of massive copper (0.7GPa).[36] The microhardness of sintered titanium (2.7GPa) corresponds to that of massive titanium, which ranges 2–3.5GPa depending on the purity and structural state.[37,38] There's a similar correspondence between the microhardness of the sintered bronze samples (2.3–2.5GPa) and massive bronze (1–3GPa, depending on the structural state).[39]

Influence of electrode scanning step on sintering of the powders

Our obtained samples have a rough surface. Roughness is influenced by the powder compactibility. The compactibility of titanium and copper is high because these materials have high plasticity, and the compactibility of MA bronze is lower than that of titanium and copper due to its high hardness. This is reflected in the appearance of the samples (Figure 3): the copper and titanium samples have more expressed faces compared with the bronze sample, the faces of which are more sloping and rounded. Also, it can be seen that the roughness of the surface increases with the increase of the

scanning step (Figure 7). This can be attributed to the use of a circular electrode: with increasing scanning step not all of the powder in the poured layer is subjected to welding (some of the powder does not fall under the electrode). This is clearly visible in the sample obtained with the scanning step of 0.7mm. The size of the imprint on the surface increases from 0.3mm to 0.7mm with increasing scanning step, and approximately corresponds to the scanning step. Reduced size of the imprint is due to the overlapping of the imprints, which results in sintering a smaller amount of powder in a single act of sintering. However, very small scanning steps cannot be used for improving the quality of sintering, because when the step is decreased, a large part of the electric pulse current can pass through the previously formed spots which have low electrical resistance; this leads to a large decrease in the current density and heat generation in the powder that is being sintered. As a result, the quality of sintering can become worse. Nevertheless, we observed decreasing surface roughness and more stable porosity and hardness values with the decrease of the scanning step. Figure 5 indicates that this problem can be avoided by the proper selection of the thickness of the powder layer and the electrode pressure upon the powder.

X-ray studies of the obtained samples

The material of the powder plays a significant role in the effective welding of particles to one another, as it determines the electrical resistivity in the points of the contact between particles, and consequently the level of heat generation at the moment when the

current passes through these contacts. The degree of heating of the material during the welding of the powder particles can be judged to some extent by changes in the structure and phase composition. X-ray diffraction analysis is a well-known method for analyzing the phase composition and structure of materials.[40] Changes in the phase composition lead to the changes in the sets and intensity of diffraction lines and by their broadening one can judge the sizes of coherent scattering regions and micro distortions. Despite the small sizes of the initial powder particles, they are monophasic or heterogeneous polycrystalline aggregates. Figure 8A (top) shows the X-ray diffraction pattern of the initial copper powder, which is represented only by the lines of this phase. The size of the CSR for the copper powder determined from the line broadening analysis was about 80 nm. After sintering bottom (Figure 8) the width remains practically unchanged, which indicates low heating of the powder particles due to the high electrical conductivity of copper and low resistance in the contacts between the particles. Figure 8B (top) shows the X-ray diffraction pattern of the initial titanium powder. The diffraction pattern contains α-Ti and TiH_2 phase lines. The presence of the TiH_2 phase is due to the specifics of the powder production method - the powder was obtained by the reduction of titanium oxides with calcium hydride. The size of the CSR of α-Ti in the powder is 70 nm. After sintering, a slight broadening of the X-ray lines occurs in the titanium-based sample (Fig. 8b, bottom) due to the decrease in the size of the CSR (43nm). This may be associated with the recrystallization of the initial powder structure due to the high heating temperature. Indeed, strong heating

of the powder is indicated by the appearance of α-Ti lines, which, according to the state diagram, can form only at temperatures above 882°C.[41] Titanium has a significantly lower electrical conductivity compared to copper. In addition, weakly conductive oxide layers are easily formed on its surface. All this leads to a significant increase in electrical resistance in the contacts between the powder particles, and more intense heating of the sintered material.

Figure 8C (top) shows the X-ray diffraction pattern of MA bronze powder, where we can see strongly broadened lines of the fcc-solid solution of tin in copper Cu(Sn) (α-phase), and the traces of lines of the inter metallic compound $Cu_{17}Sn_3$ (-phase). The size of the CSR of the α-phase is 5nm. In Figure 8C (bottom) we observe that after sintering, noticeable changes in phase composition take place in the bronze-based sample compared with the initial powder. The diffraction lines of the α-phase based on copper have become noticeably narrower due to the increase of the CSR (13nm). At the same time, an increase in the content of the β-phase takes place. The phase has a wide region of homogeneity and exists in the range of temperatures above 590°C.[42] The β-phase formation is associated with the heating of the powder particles caused by the heating of the local areas in the zones of the particle contact. Subsequent rapid cooling provides the conservation of the phase due to the high heat conductivity of the rest of the volume of the sample. Bronze is characterized by a sufficiently high electrical conductivity, which is, however, considerably lower than that of pure copper.[33,34] Therefore, the heating of the bronze powder during sintering is much higher in comparison with the copper powder.
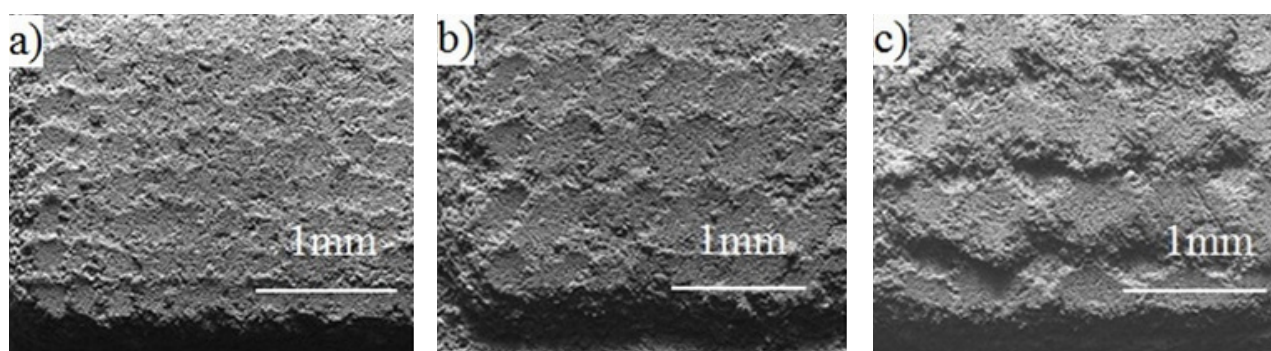

Figure 7 Electron microscope images of the surface of the copper samples sintered in steps of 0.3 mm (A), 0.5 mm (B), 0.7 mm (C).
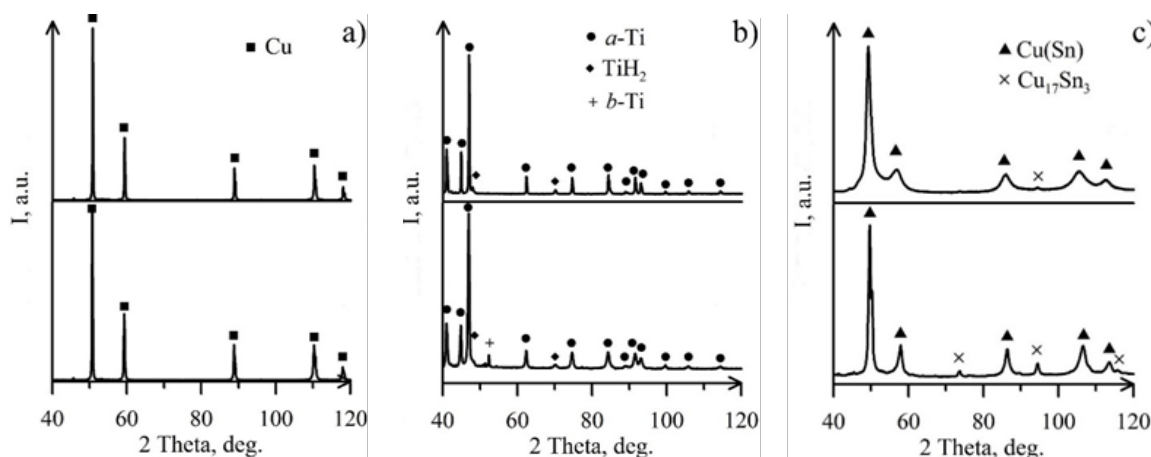

Figure 8 X-ray diffraction patterns of the initial powders of Cu(A), Ti(B) and bronze(C) (top figures), and of the samples after layer-by-layer spot PECS (bottom figures).

Discussion

In this work, we obtained consolidated samples from powders using layer-by-layer spot PECS. Obtained samples did not have any defects that are larger than the sizes of the pores between the powder particles. The powder compacts have porosity in the range of 8–35%. The observed porosity is similar to the porosity of the samples obtained by PECS,[29,30] but it is higher than the porosity of the samples obtained by LENS.[43] Despite the high porosity of the obtained sintering compacts, our method's advantage is the simplicity of its application, compared to PECS and LENS methods. Additionally, PECS method does not allow obtaining parts with the specified shape. It also should be noted that there are numerous cases when porous metal materials are required, and the method that we offer allows obtaining materials with the required level of porosity. The obtained samples have different porosity depending on the sizes and shapes of the powder particles. Small-sized particles with compact shape result in the densest packing of the particles in the powder layer spread over the substrate, and the largest number of contacts between the particles per unit of the powder volume. A large number of contacts provide the more uniform passage of current through the powder and the creation of the larger number of the points of welding between the particles. Therefore, the samples obtained from the titanium powder with small dumbbell-shaped particles are sintered with the largest density (Figures 5A & 6B). Vice versa, the number of contacts decreases between large particles and particles with an irregular shape, and thus the conditions for the formation of the powder compacts worsen. Therefore, the samples obtained from bronze and copper powders, which have large stone-shaped and dendrite-shaped particles, respectively, have high porosity (Figures 5A & 6A & 6C).

The X-ray diffraction results show that the powders with high electrical resistivity at the contacts of the particles are sintered at higher temperatures than the powder with the lower level of heat generation. The level of heat generation on the contacts and the point of melting of the material determine the sizes of the weld regions of particles. The degree of powder particle welding influences the strength of the bond between the particles. It can be observed from the microhardness of the samples (Figure 5B). For example, the low microhardness of copper-based samples indicates the incomplete consolidation of the powder particles caused by the low copper resistivity and, consequently, by the insufficient heating of the contacts between the powder particles. The agreement of the microhardness values for the samples sintered from the titanium and bronze powders and the massive materials indicates the sufficiently good coupling between the powder particles obtained as a result of sintering. The quality of the obtained sintering compacts is additionally influenced by the sintering conditions such as the thickness of the powder layer, its density, the pressure of the electrode on the powder, the scanning step, and the magnitude and duration of the electric current pulse. Therefore, for obtaining high-quality compact materials from powders using layer-by-layer spot PECS, it is necessary to optimize all the parameters of materials and the sintering process.

Conclusion

In the present paper, we tested the method for sequential point wise sintering of metal powders by pulsed electric current. The unique feature of the offered method is the use of a low-power AC source and inexpensive equipment. We demonstrate that using this method, it is possible to obtain bulk materials from metallic powders. As the powders are sintered, no warping of the obtained samples occurs.

The following patterns have been observed in the consolidation of metal powders by our method:

I. The porosity of the sintered samples mainly depends on the powder morphology. Dispersed powders with compact particles provide denser samples.

II. The powders with high electrical resistivity are consolidated with higher density because the heat generation along the boundaries of the powder particles depends on the specific resistivity of the material, as well as on the area of the contact and the transient resistance between the particles.

III. Our method is characterized by little thermal influence on the sintered powders due to the rapid process of sintering and the relatively low heating temperature of the powder particles. When the mechanically alloyed powders are sintered, the nanostructured state is retained in consolidated materials.

IV. The decrease of the electrode scanning step leads to the increase in the uniformity of the sintering compacts and the improvement of their surface quality.

Acknowledgments

Conflicts of interest

The authors declare no conflict of interest.

References

1. Bremen S, Meiners W, Diatlov A. Selective laser melting a manufacturing technology for the future? *Laser Tech J*. 2012;9:33–38.

2. Zhang K, Liu W, Shang X. Research on the processing experiments of laser metal deposition shaping. *Optics & Laser Tech*. 2007;39: 549–557.

3. Murr LE, Gaytan SM, Ramirez DA, et al. Metal fabrication by additive manufacturing using laser and electron beam melting technologies. *J of Mat Sci & Tech*. 2012;28:1–14.

4. Thijs L, Verhaeghe F, Craeghs T, et al. A study of the microstructural evolution during selective laser melting of Ti-6Al-4V. *Acta Material*. 2010l58:3303–3312.

5. Puebla K, Murr LE, Gaytan SM, et al. Effect of melt scan rate on microstructure and macrostructure for electron beam melting of Ti-6Al-4V. *Mater Sci and App*. 2012;3:259–264.

6. Nakamoto T, Shirakawa N, Miyata Y, et al. Selective laser sintering of high carbon steel powders studied as a function of carbon content. *J of Mater Process Tech*. 2009;209:5653–5660.

7. Simchi A, Pohl H. Effects of laser sintering processing parameters on the microstructure and densification of iron powder. *Mater Sci and Eng A*. 2003;359:119–128.

8. Morgan R, Papworth A, Sutcliffe C, et al. High density net shape components by direct laser re-melting of single-phase powders. *J of Mater Sci*. 2002;37:3093–3100.

9. Asgharzadeh H, Simchi A. Effect of sintering atmosphere and carbon content on the densification and microstructure of laser-sintered M2 high-speed steel powder. *Mater Sci and Eng A*. 2005;403:290–298.

10. Di W, Yongqiang Y, Xubin S, et al. Study on energy input and its influences on single-track, multi-track, and multi-layer in SLM. *Int J Adv Manuf Tech*. 2012;58:1189–1199.

11. Rafi HK, Starr TL, Stucker BE. A comparison of the tensile, fatigue, and fracture behavior of Ti-6Al-4V and 15-5 PH stainless steel parts made by selective laser melting. *Int J Adv Manuf Tech*. 2013;69:1299–1309.

12. Bandyopadhyay A, Heer B. Additive manufacturing of multi-material structures. *Mater Sci and Eng R*. 2018;129:1–16.

13. Espana FA, Balla VK, Bose S, et al. Design and fabrication of CoCrMo alloy based novel structures for load bearing implants using laser engineered net shaping. *Mater Sci and Eng C*. 2010;30(1):50–57.

14. Krishna BV, Xue W, Bose S, et al. Functionally graded Co–Cr–Mo coating on Ti–6Al–4V alloy structures. *Acta Biomater*. 2008;4:697–706.

15. Murr LE, Gaytan SM, Martinez E, et al. Next generation orthopedic implants by additive manufacturing using electron beam melting. *Int J Biomater*. 2012;245727.

16. Zhang LC, Attar HJ. Selective laser melting of titanium alloys and titanium matrix composites for biomedical applications: a review. *Agric Eng*. 2016;18(4):463–475.

17. Balla VK, Bodhak S, Bose S, et al. Porous tantalum structures for bone implants: fabrication, mechanical and in vitro biological properties. *Acta Biomater*. 2010;6(8):3349–3359.

18. Wauthle R, Van Der Stok J, Yavari SA, et al. Additively manufactured porous tantalum implants. *Acta Biomater*. 2015;14:217–225.

19. Thijs L, Sistiaga MLM, Wauthle R, et al. Strong morphological and crystallographic texture and resulting yield strength anisotropy in selective laser melted tantalum. *Acta Mater*. 2013;61(12):4657–4668.

20. Ni J, Ling H, Zhang S, et al. Three-dimensional printing of metals for biomedical applications. *Mater Today Bio*. 2019;3:100024.

21. Zergioti I, Mailis S, Vainos N, et al. Microdeposition of metals by femtosecond excimer laser. *App Surf Sci*. 1998;127:601–605.

22. Dilberoglu UM, Gharehpapagh B, Yaman U, et al. The role of additive manufacturing in the era of industry 4.0. *Philos Med*. 2017;11:545–554.

23. Grigoriev EG, Rosliakov AV. Electro-discharge compaction of WC-Co and W-Ni-Fe-Co composite materials. *J of Mater Process*. Tech. 2007;191:182–184.

24. Anisimov AG, Mali VI. Possibility of electric-pulse sintering of powder nanostructural composites. *Combustion, explosion, and shock waves*. 2010;46:237–241.

25. Kar S, Sarma ES, Somu VB, et al. Evaluation of different consolidation methods for nano-materials. *Indian J of Eng and Mater*. 2008;15:343–346.

26. Lee WH, Hyun CY. Surface characteristics of self-assembled microporous Ti-6Al-4V compacts fabricated by electro-discharge-sintering in air. *Appl Surf Sci*. 2007;253:4649–4651.

27. Lee WH, Park JW, Puleo DA, et al. Surface characteristics of a porous-surfaced Ti-6Al-4V implant fabricated by electro-discharge-compaction. *J of Mater Sci*. 2000;35:593–598.

28. Alitavoli M, Darvizeh A. High rate electrical discharge compaction of powders under controlled oxidation. *J of Mater Process Tech*. 2009;209:3542–3549.

29. Rock C, Qiu J, Okazaki K. Electro-discharge consolidation of nanocrystalline Nb-Al powders produced by mechanical alloying. *J of Mater Sci*. 1998;33:241–246.

30. An B, Oh NH, Chun YW, et al. echanical properties of environmental-electro-discharge-sintered porous Ti implants. *Materials Letters*. 2005;59:2178–2182.

31. Kim DK, Pak HR, Okazaki K. Electrodischarge compaction of nickel powders. *Mater Sci and Eng A*. 1988;104:191–200.

32. Wu X, Guo J. Effect of liquid phase on densification in electric–discharge compaction. *J Mater Sci*. 2007;42:7787–7793.

33. Malkov MP. Handbook of the physical and technical basics of cryogenics. Moscow. Energoatomizdat; 1985.

34. Mikryukov VE. Thermal conductivity and electrical conductivity of metals and alloys. Gos. Sci. and Tech. Publ. House for Ferrous and Non-Ferrous Metallurgy; 1955.

35. Shelekhov EV, Sviridova TA. Programs for X-ray analysis of polycrystals. *Metal Sci and Heat Treat*. 2000;42:309–313.

36. Valeeva AK, Valeev IS. On the microhardness and microstructure of copper Cu99,99% at radial-shear rolling. *Letters on Materials*. 2013;3:38–40.

37. Khlebnikova YV, Egorova LY, Pilyugin VP, et al. Evolution of the structure of a-titanium single crystal under severe plastic deformation by torsion under pressure. J of Tech Phys. 2015;85:60-68.

38. Kamyshanchenko NV, Nikulin IS, Kuznetsov DP, et al. Regularities of change in microhardness of technically pure titanium exposed to various mechanical and thermal effects. *Sci Bulletin Series Math Phys*. 2010;11:78–87.

39. Komkov VG, Stariyenko VA. Physical and mechanical properties of alloyed copper and tin bronze. *Sci Notes TOGU*. 2013;4:1322–1329.

40. Warren BE. X-ray diffraction. New-York. Dover Publ Inc; 1990.

41. San-Martin A, Manchester FD. The H−Ti (Hydrogen-Titanium) system. *Bulletin of Alloy Phase Diagrams*. 1987;8:30–42.

42. Saunders N, Miodownik AP. The Cu-Sn (Copper-Tin) system. *Bulletin of Alloy Phase Diagrams*. 1990;11:278–287.

43. Kruth JP, Mercelis P, Vaerenbergh J, et al. Binding mechanisms in selective laser sintering and selective laser melting. *Rapid Prototyping J*. 2005;1:26-–36.